Coastal and Offshore Science and Engineering

Numerical Modeling of Armor Layer Damage and Core Stone Erosion

M. Strazzella[a,*] and N. Kobayashi[b]
[a]*Saipem S.p.a., Italy*
[b] *University of Delaware, Newark, Delaware, USA*

[*]*Corresponding author: Michele Strazzella, Saipem S.p.a, mic.strazzella@gmail.com*

ABSTRACT: Rubble mound breakwaters are widely used for coastal protection, yet the coupled processes of armor layer damage and core stone erosion under irregular waves remain insufficiently understood. This study extends the cross-shore numerical model CSHORE to predict both armor damage progression and core crest lowering, using laboratory experiments as calibration and validation. Wave flume tests were performed on double-layer and single-layer rubble mound structures subjected to long-term irregular wave action. The double-layer breakwater experienced gradual crest lowering and exposure of core stones without their removal, whereas the single-layer structure suffered severe erosion and visible core stone loss. The numerical model was calibrated by adjusting the critical stability number for armor stone movement to account for armor layer thickness and stone interlocking. A resistance parameter representing the erosional resistance of core stones was calibrated to capture the initiation and progression of core erosion beneath a thinned armor layer. Comparisons between measured and computed profiles demonstrated that the extended CSHORE model reproduces the temporal evolution of armor damage and core erosion, though lateral scattering of dislodged stones remains unresolved. Results highlight the resilience of double-layer armor systems in delaying core exposure and preventing core stone removal compared to single-layer configurations. The proposed model provides a useful framework for evaluating the remaining capacity of damaged rubble mound breakwaters and for supporting the design of more resilient coastal defenses under climate change and storm intensification.

KEYWORDS: rubble mound, armor damage, core erosion, numerical modeling, CSHORE, wave flume

ARTICLE IN PRESS —— **DOI: 10.53256/COSE_260102**

1 INTRODUCTION

Rubble mound breakwaters consist of piles of stones composed of smaller stone for the core and larger stones for the armor layer. These structures are widely used for protecting coastlines from erosion, and for minimizing wave energy in harbor areas. These coastal structures may need to be upgraded under the threat of accelerated sea level rise and storm intensification. Design formulas were proposed to predict the damage of the armor layer but the interaction between armor and core stones during the damage progression has been investigated little. A model is developed to predict the armor layer damage and core stone erosion.

Strazzella and Kobayashi (2022) investigated the remaining capacity of a damaged rubble mound structure in a laboratory experiment, providing valuable data of armor layer and core interaction of low crested breakwaters. Two different structures were tested for a double armor layer and a single armor layer. The double-layer rubble mound was exposed to incident wave action for 22.2 hours, resulting in damage of the armor crest and exposure of core stones through the thinned armor layer without their removal. The single-layer rubble mound was exposed to incident waves for 7.8 hours. The single-layer structure was severely damaged, and some of visible core stones were removed. The numerical model CSHORE (Kobayashi, 2016) is extended in this study to predict the armor layer damage and core crest lowering under irregular waves. The experimental data were used to calibrate the numerical model. The critical stability number of armor stone movement is adjusted to account for the thickness of the armor layer and different stone interlocking. The resistance parameter of the core stones against erosional work by breaking waves is introduced in CSHORE to predict the core stone surface erosion underneath the thinned armor layer.

2 EXPERIMENT

The experiment was conducted in a wave flume that was 23 m long, 1.15 m wide, and 1.5 m high as shown in Fig. 1 (Strazzella and Kobayashi 2022). The sand beach consisted of well-sorted fine sand with a median diameter of 0.018 cm. The sand and stone characteristics are listed in Table 1.

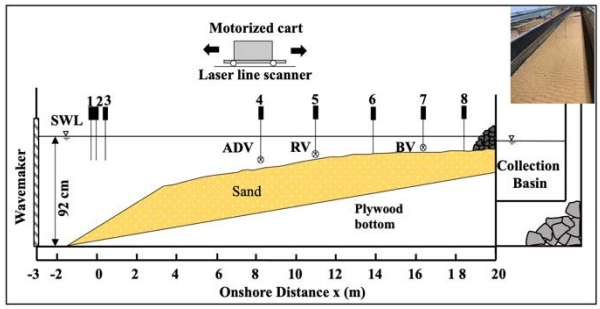

Figure 1: Experimental setup at start of the N test with no structure in the flume as shown in the inserted photo

Each run lasted 400 seconds with irregular waves of a Taxel, Marsen, and Arsloe (TMA) spectrum generated by a piston-type wave maker in water depth of 92 cm on a horizontal concrete bottom. The spectral significant wave height was 0.2 m and the peak period was 2.6 s. A relatively wide surf zone was created seaward of a large rock mound in front of the impermeable vertical wall of the collection basin for wave overtopping. No wave overtopping of the vertical wall was observed during the entire experiment.

Table 1: Characteristics and photo of sand, white stone, green stone, blue stone, and combined (green plus blue).

Parameter	Sand	White Stone	Green Stone	Blue Stone	Green and Blue
Diameter (cm)	0.018	2.11	3.52	3.81	3.65
Density (g/cm^3)	2.60	2.70	2.94	3.06	3.00
Porosity	0.4	0.44	0.44	0.44	0.44

The water surface elevation was measured by eight wave gauges, WG1-WG8 in Fig. 1. The onshore coordinate x starts from $x = 0$ at WG1 and extends to $x = 18.3$ m at WG8. The vertical coordinate z is positive upward with $z = 0$ at still water level (SWL) of 0.92 m depth. Wave gauges

DOI: 10.53256/COSE_260102

WG1, WG2, and WG3 were used to separate incident and reflected waves. WG4 and WG5 were located inside the surf zone. WG6 was placed at x = 13.8 m where the toe of the rubble mound was placed in the tests with the structure. WG7 and WG8 were used to measure the transmitted waves in the structure tests. The fluid velocities were measured at an elevation above the bed of one-third of the local water depth by one acoustic Doppler velocimeter (ADV) and two Vectrinos indicated in Fig. 1 as RV and BV. A laser scanner system, mounted on a motorized cart, was used to measure the beach profile. Three-dimensional scanned bathymetry was averaged alongshore to obtain the average cross-shore beach profile.

Three tests were performed as summarized in Table 2. Initial profiles at the beginning of each of the three tests are showed in Fig. 2. The first test was the No structure test (N test) in Fig. 2. The initial beach profile was exposed to 20 runs where the numeral after N corresponds to the run number. Each run lasted 400s and contained more than 200 waves.

Table 2: Sequence of the N, D, and S tests consisting of 310 runs with each run lasting 400s.

Test	*Runs*	*SWL (cm)*	*Duration (s)*
No structure	N1-20	0	8,000
Double armor layer	D1- 150	0	60,000
After SWL lowering	D151 - 200	-2	20,000
after D structure removal	D201 - 210	0	4,000
Single armor layer	S1 - 70	0	28,000
after S structure removal	S71 - 80	0	4,000

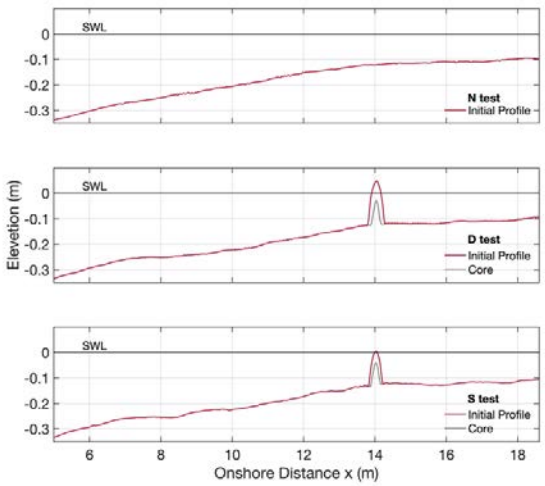

Figure 2: Initial profiles of No structure (N), Double-layer (D), and Single-layer (S) tests

The double armor layer rubble mound for the D test was built on the N20 profile at the location x = 13.74- 14.28 m. A fabric mesh with an opening of 0.074 mm was placed to avoid sand filtering through the stones (Fig. 3). The core built of white stones of D_{n50} = 2.11 cm was protected by two layers of green and blue armor stones with D_{n50} = 3.65 cm in Fig. 3 shows the initial profiles and photos of the armor, core, filter and sand surfaces before the start of the D test. The initial mound crest of the profile D0 was at the elevation z = 4.9 cm. The crest was lowered z = 0.4 cm after 150 runs. The SWL was lowered by 2 cm during D151-D200 (see Table 2.) so as to increase wave action on the crest.

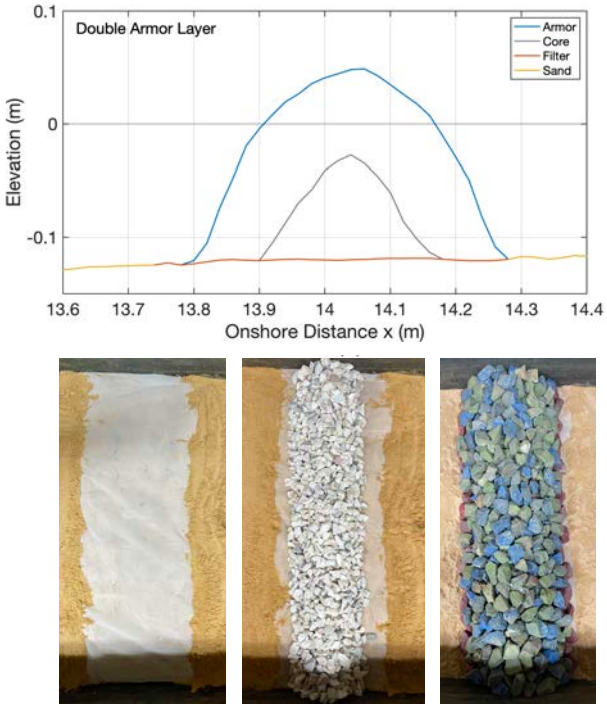

Figure 3: Initial rubble mound profile in the D test with photos depicting the placement sequence of filter (left), core (middle), and double armor layer (right) (green and blue combined in Table 1).

After the D test, the sand profile was rebuilt to be almost the same as the profile N20. The mound with a single armor layer was placed at the same location as in the D test as depicted in Fig. 4. The same filter and core were used for the single (S) armor layer structure built of the green stone of 3.52 cm nominal diameter (Table 1). For the S test, 70 runs were performed with the structure.

DOI: 10.53256/COSE_260102

Wave transformation was measured during S71-S80 with no structure (Table 2). The initial crest elevation was z = 0.5 cm for the profile S0. The crest of the final profile S70 was lowered to z = -3.3 cm and the white stones were visible through the eroded single armor layer at the end of the S test.

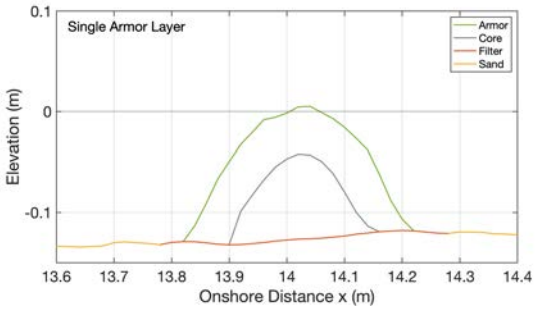

Figure 4: Initial rubble mound profile in the S test with photos depicting the placement sequence of filter (left), core (middle), and single armor layer (right) (green stone in Table 1).

3 NUMERICAL MODEL

The measurements of the N, D, and S tests were analysed and synthesized by Strazzella and Kobayashi (2022). This study compares the analysed data with the cross-shore model CSHORE (Kobayashi 2016). The version for normally incident waves was used for the comparison with the wave flume experiment. The cross-shore model consisted of the following components: a combined wave and current model based on the time-average equations of continuity, momentum, wave action, and roller energy equations; a sediment transport model for bed load and suspended load coupled with the continuity equation of bottom cohesionless sediment (sand or stone); a permeable layer model to account for porous flow inside a rubble mound; and a probabilistic swash model on impermeable (sand) and permeable (stone) bottoms above the still water level. The present CSHORE cannot predict sand beach evolution and stone structure damage simultaneously. The computation of the beach profile evolution is performed separately for the sand zone seaward of the D and S structures in Fig. 2. The computations for the D and S structures are explained in the following.

Kobayashi and Kim (2017) extended CSHORE to predict sand transport on and inside a fixed stone structure. CSHORE was applied to laboratory and prototype structures constructed of armor stones only (Yuksel and Kobayashi 2020, 2022) to predict sand transport on and inside porous stone structures.

The D and S tests in Fig. 3 and Fig. 4 were conducted to examine the remaining capacity of low-crested rubble mounds because core stones were presumed to be removed quickly after their exposure to wave action.

The core stones erosion underneath the deforming armor layer is predicted by modifying the dike erosion model proposed by Kobayashi and Weitzner (2015) which was extended to consolidate cohesive bottom erosion underneath mobile sand particles by Kobayashi and Zhu (2020). The surface elevations of the armor and core stones are denoted as z_b and z_p, respectively (Fig. 3 and Fig. 4). In the zone of no core stone, z_p is taken as the filter (assumed fixed) elevation between the armor stone and sand. The armor layer thickness hp is expressed as

$$h_p(t,x) = \left[z_b(t,x) - z_p(t,x)\right] \geq 0 \quad (1)$$

where z_b and z_p vary with time t and onshore coordinate x. The initial profiles $z_b(x)$ and $z_p(x)$ at t = 0 are input to CSHORE. The vertical erosion depth E below the initial core surface is defined as

$$E(t,x) = \left[z_p(t=0,x) - z_p(t,x)\right] \geq 0 \quad (2)$$

where E = 0 at t = 0, and E is zero or positive because of the assumption of no deposition of the eroded core stones on the stone surfaces of z_b and z_p as observed in the experiment.

The conservation equation of armor stone volume per unit horizontal area on the core stone surface z_p is given by

$$\left(1-\eta_p\right)\frac{\partial h_p}{\partial t} + \frac{\partial q_x}{\partial x} = 0 \quad (3)$$

where the stone porosity $\eta_p = 0.44$, and the cross-shore sediment (armor stone) transport rate q_x (no void) is estimated using the formulas for bed load and suspended load (practically zero for armor stone) in CSHORE (Kobayashi 2016).

DOI: 10.53256/COSE_260102

The core stone erosion depth E is computed using the following equation based on the rate of erosion work

$$\rho R \frac{\partial E}{\partial t} = FD \qquad (4)$$

where the fluid density ρ is added to express the core stone resistence force ρR per unit area. The resistance parameter R is proportional to the velocity squared. The energy dissipation rate D per unit area for the core stone erosion is estimated using the computed wave energy dissipation rates due to wave breaking and bottom friction in CSHORE. The bottom slope effect is included for the steep side slope of D and S mounds (Fig. 3 and Fig. 4). The dimensionless function F was introduced by Kobayashi and Zhu (2020) to account for the abrasive effect of a thin mobile sand layer on the erosion of consolidated cohesive bottom as well as the protective effect of a thick sand layer. The abrasive effect of mobile armor stone is neglected because its movement was infrequent. For the case of no protective effect, F=1 and the energy dissipation rate D is utilized for the rate of erosion work on the left-hand side of Eq. (4). The protective effect of the armor layer should reduce the portion of D transmitted to the core stone through the armor layer thickness h_p. The function of F is tentatively assumed to be expressed as

$$F = \exp(-3h_*)\,;\; h_* = h_p/D_{n50} \qquad (5)$$

which yields F=1 for h_p=0 and no protective armor layer. The nominal armor stone diameter D_{n50} (Table 1) is used to normalize h_p. The value of h_* is one (two) for single (double) armor layer. The value of F decreases by a factor of 20 from h_*=1 to h_*=2.

The core stone resistance parameter R needs to be specified as input. The calibrated values of full-scale dike testing were 1,000 and 200 $(m/s)^2$ for good (dense roots) and poor grass covers, respectively, and 10 $(m/s)^2$ for boulder clay with a network of cracks formed under long-term weathering (Kobayashi and Weitzer 2015). The value of R = 10 $(m/s)^2$ is used for the core stone in the D and S tests. For the landward and seaward zones of no core stone at t=0, R= 10,000 $(m/s)^2$ was specified as input to represent the filter and the sand surface which were assumed immobile for the computation of armor stone damage and core stone erosion. Erosion underneath the filter is not predictable and was neglected.

Eqs. (1) – (5) were solved numerically to compute the temporal and cross-shore variations of z_b, z_p, h_p, and E using the measured time series of the still water level (SWL), spectral significant wave height H_{mo}, peak period T_p, and wave setup $\bar{\eta}$ above the SWL at the seaward boundary of the computational domain. The computational procedure was explained by Kobayashi and Zhu (2020) who computed sand transport and erosion of consolidated cohesive bottom containing sand. The sand and cohesive sediment were replaced by the armor stone and core stone in the stone computation. For the computation of the beach profile evolution, the sand characteristics (Table 1) were specified as input. The computation domain starting from x=0 ended at x=18.6m for the N test and at x=13.7m for the D and S tests in Fig. 2. So that there was no rubble mound structure in the sand computation domain. The cross-shore nodal spacing was 2 cm for all the computations. The input parameters for CSHORE (Kobayashi 2016) were taken as standard values unless stated otherwise in the following comparisons for each test.

4 NO (N) STRUCTURE TEST

For the N test the computation domain was chosen from x=0 at WG1 to x=18.6 m at the toe of the rock slope in front of the vertical wall in Fig. 1. The suspension load parameter in the CSHORE input was increased from 0.2 to 0.4 to increase offshore suspended sand transport and the computed height of the bar crested in the outer surf zone. The measured H_{mo}, T_p, and $\bar{\eta}$ for the incident waves at WG1 were specified as input. The incident waves were allowed to propagate landward at x = 18.6 m. Reflected waves from the rock slope were neglected. The wave reflection coefficient measured at x=0 was 0.14 (Strazzella and Kobayashi 2022) but wave reflection was not measured at x=18.6 m inside the surf zone where linear wave theory may not be reliable.

Fig. 5 shows the initial measured profile N0, the measured profile N20 which was almost equilibrium, and the computed profile N20. The measured initial profile N0 was eroded in the zone of x = 8-14m. A small bar was detected in the zone of x = 6-8 m. CSHORE predicts the initiation of the bar at the edge of the outer surf zone, but the computed bar location was in the zone of x=5-7m.

DOI: 10.53256/COSE_260102

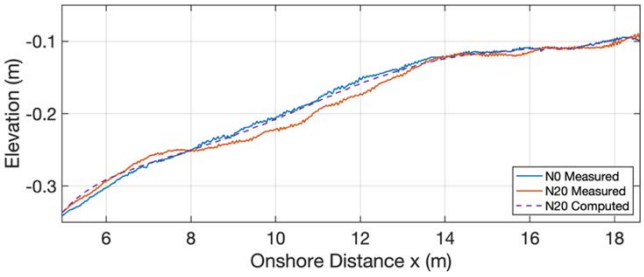

Figure 5: Initial profile (N0) and measured and computed final profiles (N20) where the numeral after N indicates the number of runs with each run lasting 400s.

The measured and computed averaged values of the mean and standard deviation of the free measured surface elevation η and horizontal velocity u are compared for the intervals of N1-N10 and N11-N20 in Fig. 6. The spectral significant wave height H_{mo} and peak period T_p of the incident waves at $x = 0$ were 21 cm and 2.6 s, respectively. The mean free surface elevation $\bar{\eta}$ (wave setdown or setup) is predicted reasonably except for the overprediction in the inner surf zone. The free surface standard deviation σ_η related to the local significant wave height $H_{mo}= 4\sigma_\eta$ is somewhat underpredicted in the inner surf zone. The mean horizontal velocity is negative because of the offshore return flow and predicted well. The standard deviation σ_u of the wave-induced oscillatory velocity is predicted fairly.

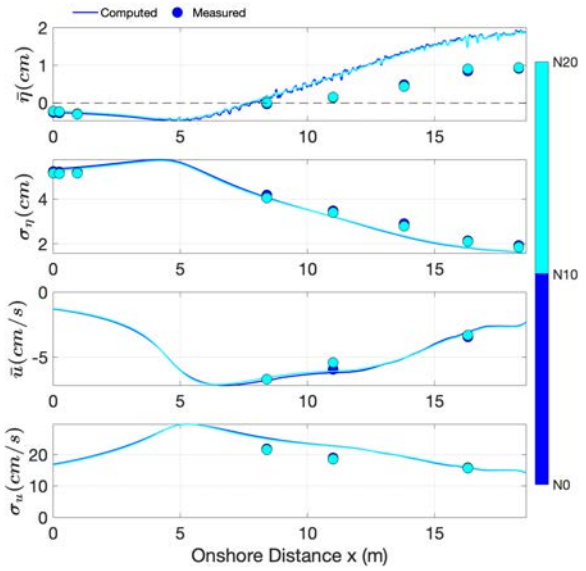

Figure 6: Measured and computed average values of mean and standard deviation of free surface elevation η and cross-shore velocity u for N1-N10 and N11-N20 runs in the N test.

5 DOUBLE (D) LAYER TEST

The D test mound was built on the beach profile N20 in the zone x = 13.74 – 14.28 m and exposed to 200 runs of 400s waves (Table 2). The evolution of the rubble mound and adjacent beach profile was measured 18 times from the profile D0 to the final profile D200 (Fig. 7). The initial mound deformation was caused by the dislocation of stones placed in unstable positions. The dislocated stones became more stable in their new positions. Offshore sand transport resulted in the formation of a bar near x = 7m and deposition extending to the zone of x < 5m with no profile measurement by the motorized cart in Fig. 1. The initial profile between x=0-5 m was assumed linear for the profile evolution computation.

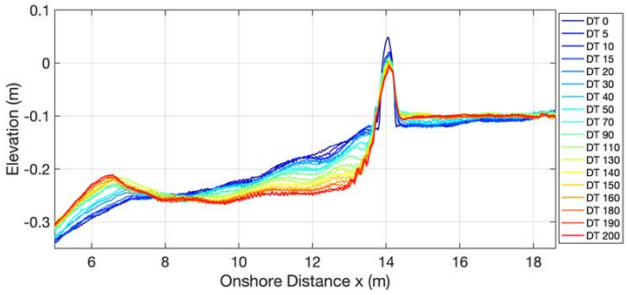

Figure 7: Measure 18 profiles starting from the initial profile (D0) to the final profile (D200) in the D test.

For the numerical simulation the domain of x = 0.0-18.6m was separated to the sand zone of x = 0.0-13.7m and the stone computation zone of x = 13.7-18.6m. The toe of the D mound was located at x = 13.8 m in Fig. 3. The sand zone computation was performed in the same way as in the N test using the suspend load parameter of 0.4 to increase the bar height by about 30% (in Fig. 8). CSHORE cannot predict the measured trough deepening sufficiently. Fig. 9 shows the measured and the computed bar crest heights increasing with the number of runs. CSHORE predicts the temporal increase of the bar crest height, but the predicted bar location is too seaward. This discrepancy may be related to sand transport under irregular breaking waves in the outer surf zone.

DOI: 10.53256/COSE_260102

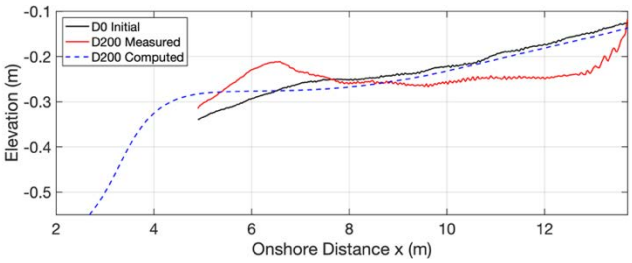

Figure 8: Measured and computed final profiles (D200) starting from the initial beach profile (D0) where x =5m was the seaward limit of the motorized cart movement in Fig. 1.

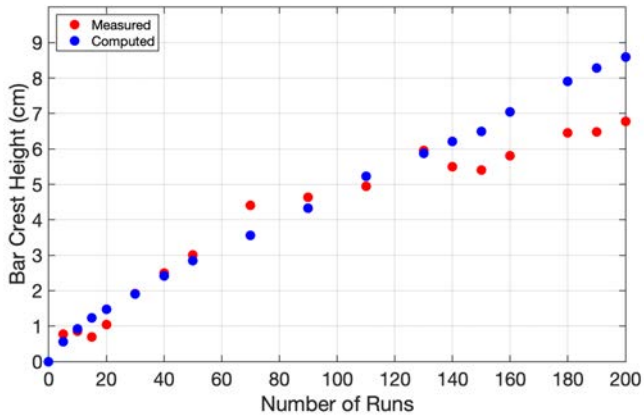

Figure 9: Measured and computed bar crest heights above the initial profile increasing with the number of runs during the D test.

For the design of coastal structures, incident waves are normally specified at the toe of the structure (Burchart et al. 2006). The measured values of H_{mo}, T_p, and $\bar{\eta}$ at WG6 located at x=13.8m in Fig. 1 are specified at x = 13.7m as input to CSHORE where the seaward shift of 0.1m was based on the seaward deposition of displaced armor stones during the D test. The measured values of H_{mo} during 10 runs before and after the mound removal in the D test (Table 2) were compared to estimate the effect of reflected waves from the mound. The values of H_{mo} decreased 5% after the mound removal. The small reflected wave effect was neglected in the CSHORE computations.

Fig. 10 compares the measured and computed final armor stone profiles (D200) in view of the initial profile (D0). The critical stability number Nc for the initiation of stone movement (Kobayashi et al. 2010) is calibrated as Nc = 1.4 for the D test. The agreement of the measured and the computed profiles demonstrates the CSHORE capability of simulating the cross-shore stone movement on the steep side slope of the rubble mound.

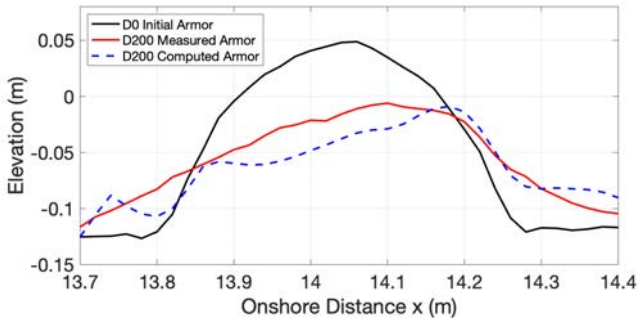

Figure 10: Measured and computed final armor stone profile (D200) starting from the initial armor profile (D0).

Fig. 11 presents the progression of armor layer damage S over time, expressed as the eroded area divided by D_{n50}^2, with D_{n50} = 3.65cm in the D test. CSHORE cannot predict the initial damage of casually placed stones but the agreement between the measured and computed damage becomes reasonable after the damage exceeds about 8.

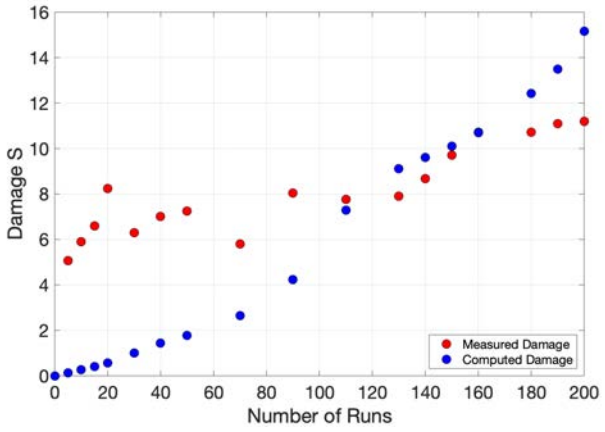

Figure 11: Measured and computed armor layer damage (normalized eroded area) during the D test with the nominal stone diameter Dn50=3.65cm.

Fig. 12 depicts the measured and computed armor layer erosion depth normalized by D_{n50} = 3.65cm. The stability number N_{mo} based on the H_{mo} at the toe of the structure remained between 1.65 and 1.91 during the D test. Fig. 11 and Fig. 12 imply that the temporal changes of the eroded area and depth were similar under the wave action which remained fairly constant. The armor stones should have been placed more carefully to reduce the initial damage.

DOI: 10.53256/COSE_260102

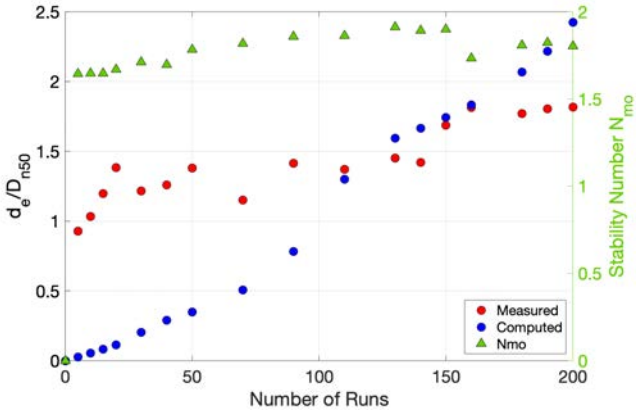

Figure 12: Measured and computed armor layer erosion depth de normalized by Dn50=3.65cm and stability number Nmo based on Hmo at WG6, varying with the number of runs during the D test.

CSHORE has been extended in this study to core stone erosion underneath the damaged armor layer. After D200 the armor stones were manually removed, and the core stone surface was measured with the laser scanner. The measured and computed final core profiles (D200) are compared with the initial core profile (D0).

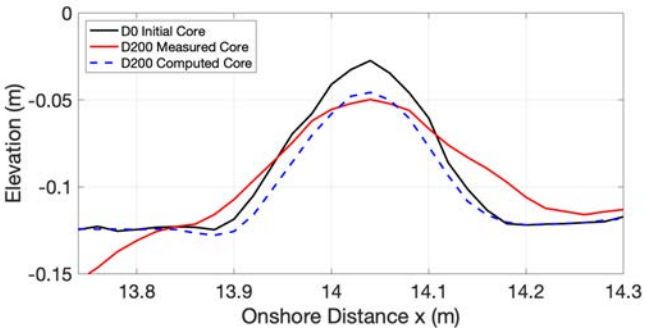

Figure 13: Measured and computed final core stone profiles (D200) starting from the initial core profile (D0).

The simple core erosion model based on Eqs. (4) and (5) predicts the core mound crest erosion and lowering (Fig. 13) but does not predict the scattering of dislodged armor and core stones (Fig. 14). The actual damage progression of discrete armor and core stones in Fig. 14 was highly complex.

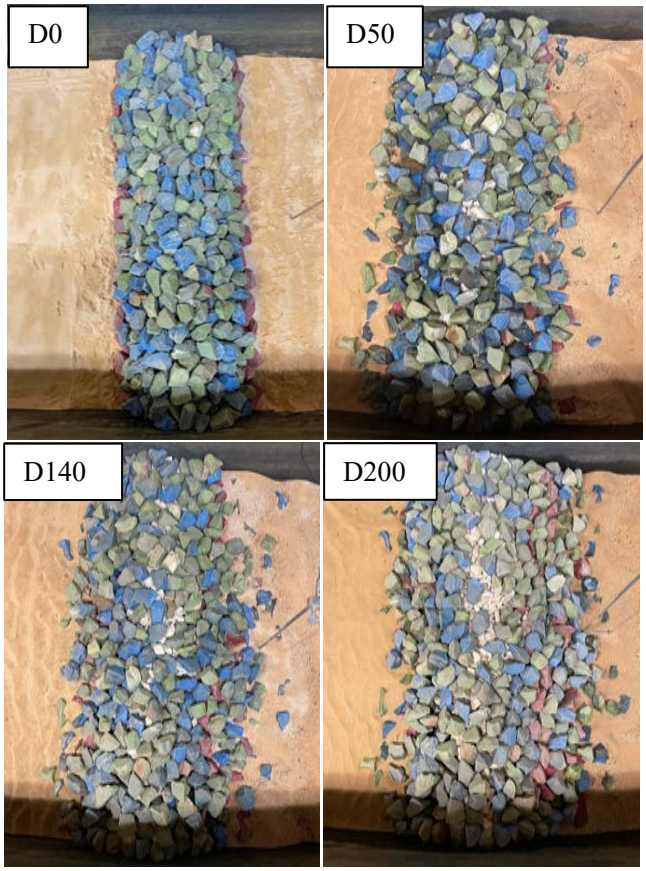

Figure 14: Photographic damage progression starting from the intact armor layer (D0), visible white core stones (D50), gradual enlargement of white stone holes (D140), and the final armor layer with fairly stable white stone holes (D200).

6 SINGLE (S) LAYER TEST

The S test mound was constructed on the equilibrium beach profile N20, re-built after the D Test. The rubble mound was placed at x = 13.74–14.28 m as shown in Fig. 15. A single layer of Green armor stones (Table 1) was placed atop the core of White stones. Irregular waves (H_{mo} = 0.2 m, T_p = 2.6 s) were applied for 70 runs (28,000 s), followed by removal of the armor layer and measurement of wave transformation over runs S71–S80 (Table 2). Laser-scanned cross-shore profiles were recorded 11 times from the initial profile S0 (crest at z = 0.01m) to the final profile S70 (crest lowered to z = –0.07 m).

DOI: 10.53256/COSE_260102

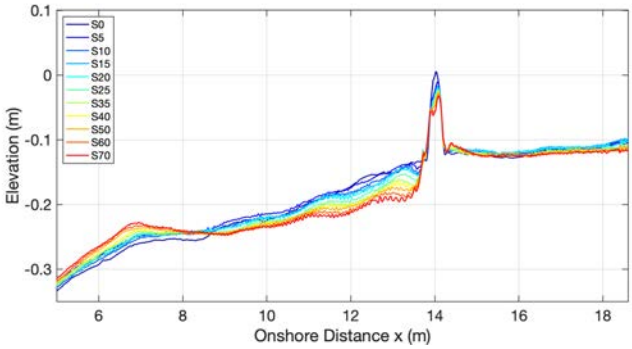

Figure 15: Measured 11 profiles starting from the initial profile (S0) to the final profile (S70) in the S test.

For numerical simulation, the domain was partitioned into a sand zone (x = 0.0–13.7 m) and a stone zone (x = 13.7–18.6 m), with the toe of the S mound at x = 13.8 m.
Sand transport in the sand zone was computed as in the N test. Fig. 16 compares the measured and computed final beach profiles (S70) starting from S0. CSHORE reproduces the offshore bar formation but underestimates the trough deepening as in Fig. 16, suggesting limitations in modelling sand transport under irregular breaking waves.

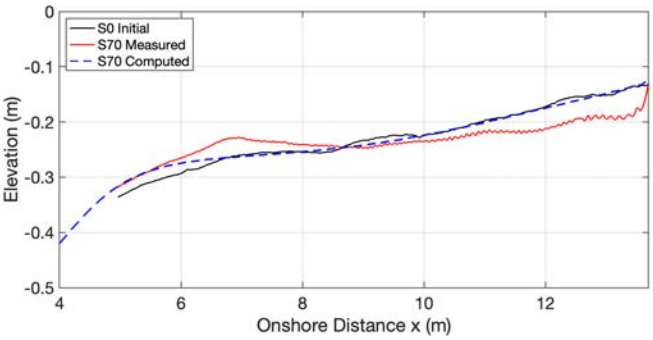

Figure 16: Measured and computed final profiles (S70) stating from the initial beach profile (S0).

Fig. 17 shows the temporal evolution of bar crest height, with CSHORE mimicking the bar growth rate.

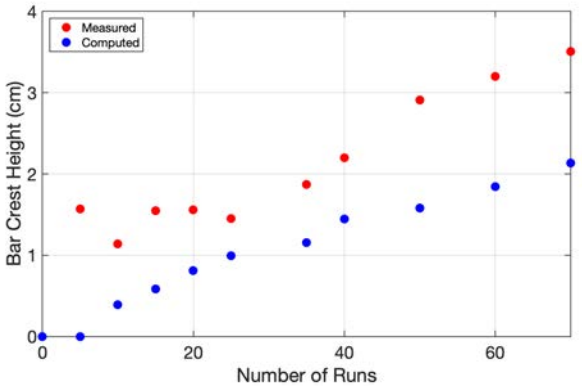

Figure 17: Measured and computed bar crest heights above the initial profile increasing with the number of runs during the S test.

Fig. 18 presents the measured and computed final armor stone profiles for S70 versus the initial profile S0. The critical stability number *Nc* was reduced to 0.5 from *Nc*=1.4 of the D test to reduce the crest lowering and slope flattening. The calibrated *Nc* = 0.5 yields close agreement of crest lowering and side-slope deformation, demonstrating CSHORE's capability to simulate stone movement on steep slopes.

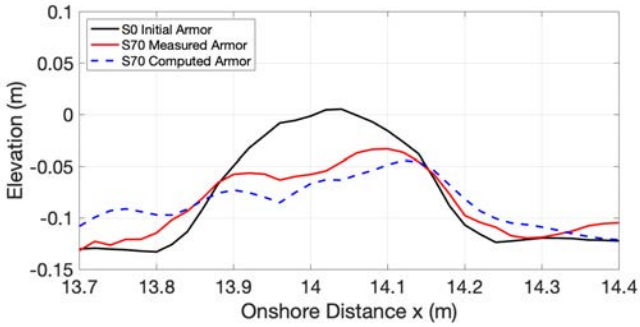

Figure 18: Measured and computed final armor stone profiles (S70) starting from the initial armor profile (S0).

Fig. 19 traces the normalized armor layer damage against run number, expressed as the eroded area divided by D_{n50}^2, with D_{n50} = 3.52cm in the S test. The numerical model successfully captures the early phase of damage progression, particularly up to run 20, where the predicted damage aligns closely with experimental data. Beyond run 20, however, the model slightly underpredicts the damage accumulation compared to the measured values. Despite this limitation, the model captures the overall trend and magnitude of erosion depth and damaged area throughout the test duration.

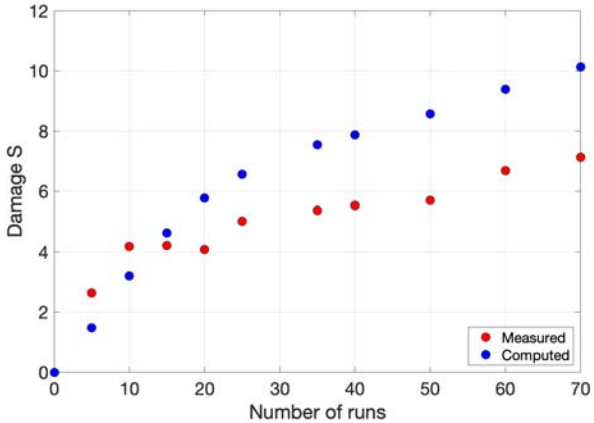

DOI: 10.53256/COSE_260102

Figure 19: Measured and computed armor layer damage (normalized eroded area) during the S test with the nominal stone diameter Dn50=3.52cm.

Fig. 20 presents the temporal evolution of measured and computed armor layer erosion depth normalized by D_{n50} = 3.52cm where the stability number N_{mo} based on the H_{mo} at the toe of the structure remained between 1.6 and 1.79 during the S test.

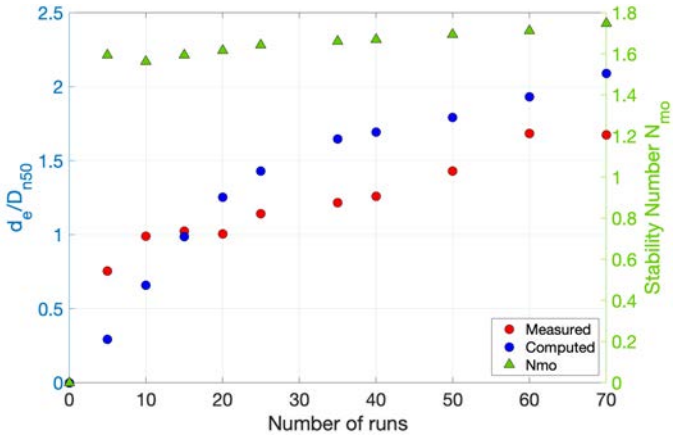

Figure 20: Measured and computed armor layer erosion depth de normalized by Dn50=3.52cm and stability number Nmo based on Hmo at WG6, varying with the number of runs during the S test.

After armor removal, the core stone profile was measured and compared in Fig. 21. The core crest lowering is well predicted, confirming the limitation of single-layer thickness for core protection. However, the model cannot reproduce the lateral scattering of dislodged stones. Fig. 22 illustrates the actual damage progression of the gradual enlargement of the exposed stone area.

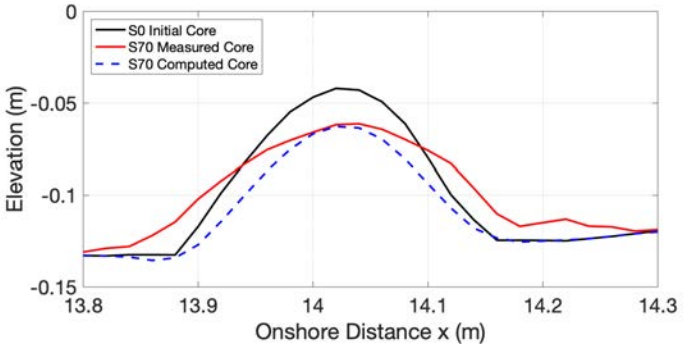

Figure 21: Measured and computed final core stone profiles (S70) starting from the initial core profile (S0).

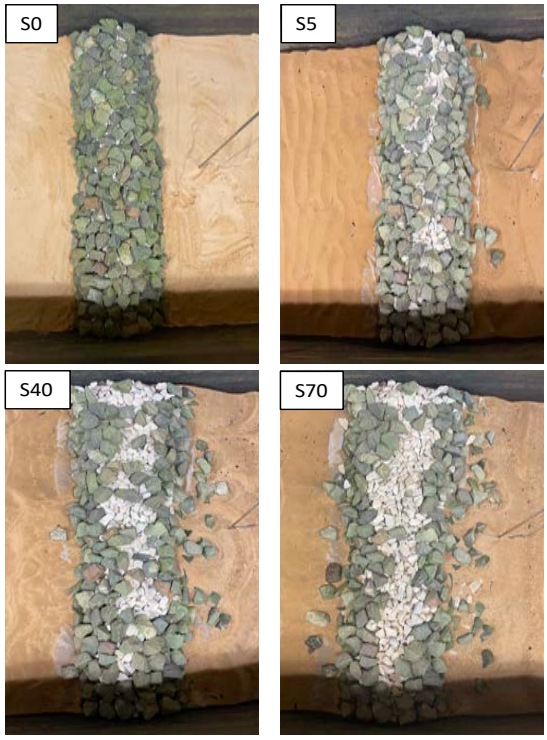

Figure 22: Photographic damage progression starting from the intact armor layer (S0), visible white core stones (S5), gradual enlargement of white stone holes (S40), and the final armor layer with dislodged stones (S70).

7 CONCLUSIONS

This study advances the predictive modeling of rubble mound breakwaters by extending the CSHORE numerical model to simulate both armor layer damage and core stone crest lowering under irregular wave loading. Calibration against wave-flume experiments allowed for the adjustment of the critical stability number (N_c) to reflect the influence of armor layer thickness and stone interlocking, N_c= 1.4 for the double-layer structure (D test) and N_c=0.5 for the single-layer structure (S test). The core stone resistance parameter was set at R = 10 $(m/s)^2$, effectively capturing the observed onset and progression of core erosion.

Results demonstrate that the double-layer breakwater exhibited gradual crest lowering with core exposure but no removal of core stones, while the single-layer structure experienced severe erosion and significant core stone loss.

DOI: 10.53256/COSE_260102

These findings highlight the critical protective role of double armor layers and the complexity of the coupled evolution of armor and core stone layer.
Overall, the calibrated CSHORE model provides a valuable tool for the assessment and design of resilient rubble mound breakwaters, supporting effective coastal adaptation strategies in the face of climate change and increasing storm intensity.

8 ACKNOWLEDGEMENTS

This work was supported by HR Wallingford, which sponsored the presentation of part of this study at the Breakwater 2023 conference. The authors also gratefully acknowledge Saipem S.p.A. for sponsoring the participation at the International Conference on Coastal Engineering (ICCE) 2025, where the results of this study were presented orally.

9 REFERENCES

Burcharth, H. F., M. Kramer, A. Lamberti, and B, Zanuttigh. 2006. Structural stability of detached low crested breakwaters. *Coastal Eng. 53 (4): 381–394.*

Strazzella, M., and N. Kobayashi. 2022. Remaining capacity of low-crested rubble mounds damaged by breaking waves in surf zone. *Journal of Waterway, Port, Coastal, and Ocean Engineering, 2022, 148(6): 04022020.*

Kobayashi, N. 2016. Coastal sediment transport modeling for engineering applications. *Journal of Waterway, Port, Coastal, and Ocean Engineering 2016, 142 (6):03116001.*

Kobayashi, N., and H. D. Kim. 2017. Rock seawall in the swash zone to reduce wave overtopping and overwash of a sand beach. *Journal of Waterway, Port, Coastal, and Ocean Engineering, 2017, 143 (6): 04017033.*

Kobayashi, N., and H. Weitzner. 2015. Erosion of a seaward dike slope by wave action. *Journal of Waterway, Port, Coastal, and Ocean Engineering, 2015, 141, No. 2*

Kobayashi, N., and T. Zhu. 2020. Erosion by Wave Action of Consolidated Cohesive Bottom Containing Cohesionless Sediment. *Journal of Waterway, Port, Coastal, and Ocean Engineering, 2020, 146, No. 2.*

Yuksel, Z. T., and N. Kobayashi. 2020. Comparison of revetment and sill in reducing shore erosion and wave overtopping. *Journal of Waterway, Port, Coastal, and Ocean Engineering, 2020, 146 (1): 04019028.*

Yuksel, Z. T., and N. Kobayashi. 2022. Numerical modelling of revetment and sill in reducing shore erosion. *Coastal Offshore Science and Engineering. Year 1, Volume 1, 8-19.*